

# Linear Direct Current Electromagnetic Motor with Liquid Eutectic Gallium-Indium Alloy Coil

Jason Guan

27 September 2019

892594255

Department of Engineering Science  
Supervised by Dr. Bryan Ruddy

## **Abstract**

Abstract placeholder

## Acknowledgements

Paul Roberts

Steve Oldman

Greg

Nick, Suroosh, Mahsa and Yahya

And of course, Dr. Bryan Ruddy

# Contents

<b>1</b>	<b>Table of Notation</b>	<b>5</b>
<b>2</b>	<b>Introduction</b>	<b>6</b>
<b>3</b>	<b>Design, Manufacturing and Assembly</b>	<b>7</b>
3.1	Mathematical Modelling . . . . .	7
3.1.1	Motor Force . . . . .	7
3.1.2	Heat and Temperature . . . . .	9
3.2	Optimisation Algorithm . . . . .	10
3.3	Design Validation . . . . .	11
3.4	Physical Design and Manufacturing . . . . .	12
3.4.1	Shell . . . . .	12
3.4.2	Core . . . . .	13
3.4.3	Wire Bobbin . . . . .	14
3.5	Assembly . . . . .	14
3.5.1	Shell and Magnet Assembly . . . . .	14
3.5.2	Wire Assembly . . . . .	14
3.5.3	Health, Safety and Containment . . . . .	14
<b>4</b>	<b>Experiment Designs and Results</b>	<b>15</b>
4.1	Experiment 1: Force Characterisation . . . . .	15
4.1.1	Method . . . . .	15
4.1.2	Results . . . . .	16
4.2	Experiment 2: Circulation Thermoregulation . . . . .	16
4.2.1	Method . . . . .	16
4.2.2	Results . . . . .	16
<b>5</b>	<b>Discussion</b>	<b>17</b>
<b>6</b>	<b>Conclusion</b>	<b>18</b>
<b>7</b>	<b>Appendices</b>	<b>19</b>
7.1	Full Results of Motor Force Experiment . . . . .	19

# 1 Table of Notation

Symbol	Description	Units
$P_{in}$	Electrical power input	$W$
$P_{out}$	Total power output	$W$
$P_{mech}$	Mechanical power output	$W$
$P_{heat}$	Heat power output	$W$
$f$	Frequency	$Hz$
$\mathcal{F}$	Magnetomotive force	$A$
$\mathcal{R}$	Magnetic reluctance	$H^{-1}$
$\mathcal{R}_{mag}$	Magnetic reluctance of the magnet	$H^{-1}$
$\Phi$	Magnetic flux	$Wb$
$\Phi_0$	Short circuit magnetic flux, i.e. flux in circuit when poles of magnet are connected with minimal reluctance	$Wb$
$L_{Wtotal}$	Total length of wire in motor	$m$
$L_{mag}$	Axial length of cylindrical magnet	$m$
$B$	Magnetic field density	$T$
$B_r$	Residual flux density of magnet	$T$
$I$	Electric current	$A$
$d_{travel}$	Required travel distance of the motor bobbin	$m$
$c_{pWire}$	Specific heat capacity of wire	$JKg^{-1}K^{-1}$
$\mu_0$	Vaccum permeability, $4\pi \times 10^{-7} Hm^{-1}$ [1]	$Hm^{-1}$
$\mu_s$	Relative magnetic permeability of mild steel, 760 [2]	NA
$\mu_m$	Relative magnetic permeability of neodymium magnet, 1.05 [1]	NA

## 2 Introduction

Soft robotics has in recent years enjoyed a surge in research interest. Traditional robots that use rigid materials for actuation tend to have poor adaptability and low human friendliness. Robots and actuators made with mechanically compliant materials may emerge more adaptable in unpredictable conditions and more comfortable for wearable use.

Current soft robot actuation methods include chemical, pressure-based (pneumatic or hydraulic) and electroactive elastomer. Electromagnetic actuation that most traditional robots rely on has been mostly overlooked. Only four years ago, Jin et al. published [3], the first paper that explored the idea. Jin introduced a voice coil speaker effective under large deformations.

As a result, there is an opportunity add to the under-researched area of electromagnetic actuation for soft robots. Rigid electromagnetic actuation is a relatively mature field with a large existing corpus.

Previously, electromagnetic actuation in soft robots was hindered by a lack of good conductors that maintain electrical properties under large deformations. Eutectic Gallium-Indium alloys (eGaIn) have emerged as a potential solution. eGaIn is a family of alloys that contain gallium, indium and sometimes tin and other metals. A typical eGaIn alloy can have 75% Ga and 25% In and melts at 15.5 °C [4], meaning it is liquid under room temperature. Liquid metal conductors can deform without large changes to material properties and do not undergo strain hardening or fatigue.

eGaIn is also advantageous among other liquid metals in that it has low toxicity [4], compared to mercury which is highly toxic. eGaIn is also stable in atmospheric conditions, compared to sodium-potassium alloy which is pyrophoric [5], and has low vapour pressure. eGaIn does however form an oxide layer on contact with oxygen which hinders its fluid and electrical properties [6].

Using liquid metal in electromagnetic actuator coils also makes available a novel approach to cooling. The conductors themselves can be circulated and cooled externally, away from the rest of an actuator. This means that thermoregulation features such as cooling fins may become detached from the actuator, allowing for more compact designs where space is at a premium.

This project seeks to answer whether it is feasible to build an electromagnetic motor using liquid metal for wiring that can also be cooled via circulating metal in the wiring. To that end, an electromagnetic motor with eGaIn coils was designed, built and characterised. An analysis will also be conducted on whether eGaIn actuators hold promise for use in soft robots or for novel cooling approaches.

### 3 Design, Manufacturing and Assembly

#### 3.1 Mathematical Modelling

##### 3.1.1 Motor Force

$$\mathcal{F} = \mathcal{R}\Phi \quad (1)$$

Magnetomotive force of a magnet can be calculated using total magnetic reluctance in a magnetic circuit and magnetic flux in that circuit, seen in equation 1. This is analogous to electrical circuits following Ohm's law: magnetomotive force is analogous to voltage, reluctance is analogous to resistance and flux is analogous to current. Magnetomotive force in cylindrical magnets can be calculated using a short circuit scenario, i.e. by assuming poles of magnet are connected with minimal reluctance. Under the assumption that magnetic field density is uniform, the short circuit flux is equal to the remanence field density of the magnet multiplied by the cross-sectional area of the magnet normal to the direction of the magnetic field. In the case of an axially magnetised cylindrical magnet, this area is equal to the radial cross-section area of the cylinder.

$$\Phi_0 = B_r A_{mag} \quad (2)$$

Substituting equation 2 into equation 1 gives a way to simply calculate  $\mathcal{F}$  using axial length of magnet and remanent field density:

$$\begin{aligned} \mathcal{F} &= \mathcal{R}_{mag} \Phi_0 \\ &= \frac{L_{mag}}{A_{mag}} B_r A_{mag} \\ &= L_{mag} B_r \end{aligned} \quad (3)$$

The magnetic circuit of a voice coil motor travels through four components in series: the magnet, the core, the "air" gap where the coils are and the shell, seen in figure 1. This

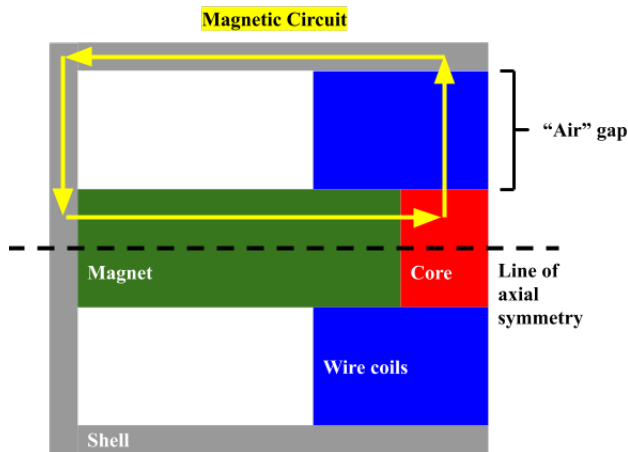


Figure 1: Simplified axisymmetric diagram of typical moving-wire voice coil motor

means the total reluctance in the circuit can be represented by equation 4, similar to how

resistance is calculated in an electrical circuit.

$$\mathcal{R}_{total} = \mathcal{R}_{gap} + \mathcal{R}_{mag} + \mathcal{R}_{core} + \mathcal{R}_{shell} \quad (4)$$

Magnetic reluctance can be calculated as the proportion of magnetic path length  $l_m$  and the product of material permeability  $\mu$  and cross-sectional area normal to magnetic flux  $A$ , seen in equation 5 [7].

$$\mathcal{R} = \frac{l_m}{\mu A} \quad (5)$$

Assuming the shell and core are made out of magnetically conductive material such as mild steel, the permeability of shell and core will be hundreds of times higher than the permeability of "air" gap and magnet [1]. Therefore, the reluctance of shell and core can be approximated to zero for the purposes of this calculation. Substituting simplified equation 4 into equation 1 produces:

$$\mathcal{F} = (\mathcal{R}_{gap} + \mathcal{R}_{mag})\Phi \quad (6)$$

Reluctance between two coaxial cylinders, in this case between the magnet and the shell, can be calculated as in equation 7, assuming all magnetic flux flows through the core [8]. Relative permeability of the gap is approximated to 1 as none of air, silicone or eGaIn are ferromagnetic [1].

$$\mathcal{R}_{gap} = \frac{\mu_0 \ln \frac{r_{out}}{r_{in}}}{2\pi L_{core}} \quad (7)$$

Reluctance through the magnet can be calculated as seen in equation 8, similar to how resistance would be calculated for a cylinder.

$$\mathcal{R}_{mag} = \frac{\mu_m L_{mag}}{2\pi r_{mag}^2} \quad (8)$$

Substituting equations 7, 8 and 3 into equation 6 gives equation 9 which yields flux in the motor magnetic circuit.

$$L_m B_r = \frac{\ln \frac{r_{out}}{r_{in}}}{2\pi L_c} \Phi$$

$$\frac{2\pi L_m L_c B_r}{\ln \frac{r_{out}}{r_{in}}} = \Phi \quad (9)$$

To calculate the magnetic field density in the "air" gap, which can then be used to calculate force acting on the moving coils, the area of action that the flux is distributed across is also required as seen in equation 10.

$$\Phi = B_{gap} A_{active} \quad (10)$$

Substituting equation 10 into equation 9 gives equation 11, which can be used to calculate

the magnetic field density  $B_{gap}$  across the "air" gap.

$$B_{gap} = \frac{2\pi L_{mag} L_{core} B_r}{\ln \frac{r_{out}}{r_{in}} A_{active}} \quad (11)$$

Using Lorentz's force law substituted with equation 11, equation 12 gives a minimum current  $I$  can be obtained given a known required force  $F$  and a known length of wire in the magnetic field  $L_{active}$ .

$$\begin{aligned} F &= B_{gap} I L_{active} \\ I &= \frac{F}{B_{gap} L_{active}} \\ I &= \frac{F A_{active} \ln \frac{r_{out}}{r_{in}}}{2\pi L_{mag} L_{core} B_r L_{active}} \end{aligned} \quad (12)$$

The active area in the magnetic field is different for each layer of wire in the motor. Layers of wire further away from the magnet, meaning a larger area and therefore lower magnetic field density. The total active area that magnetic flux is distributed across can be calculated as shown in equation 13, where  $n$  is the total number of wire layers.

$$A_{active} = \sum_1^n A_{active}^{layer} = 2\pi L_c (r_{core} - r_{wireout} + 2r_{wireout} \frac{(n+1)n}{2}) \quad (13)$$

The length of wire in the magnetic field can be calculated in a similar fashion, shown in equation 14.

$$L_{active} = L_{core} \pi (layers + 1) layers + \frac{L_{core} r_{mag} \pi}{r_{wireOut}} \quad (14)$$

Combining equations 12, 13 and 14 yields a final current calculation seen in equation 15.

$$I = \frac{F \cdot 2\pi L_c (r_{core} - r_{wireout} + 2r_{wireout} \frac{(n+1)n}{2}) \ln \frac{r_{out}}{r_{in}}}{2\pi L_{mag} L_{core} B_r L_{core} \pi (layers + 1) layers + \frac{L_{core} r_{mag} \pi}{r_{wireOut}}} \quad (15)$$

### 3.1.2 Heat and Temperature

Using heat energy can calculate temperature in wires Safety

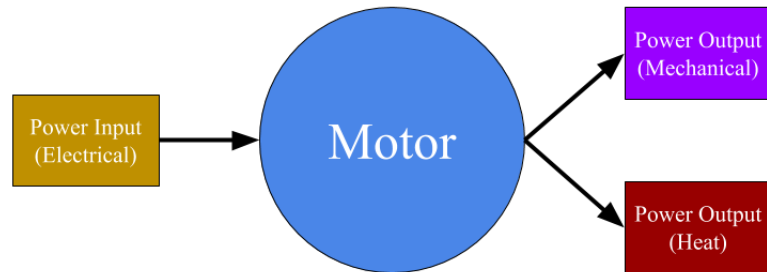


Figure 2: Conservation of energy in the motor system

$$P_{in} = IV = I^2 R \quad (16)$$

$$R = \frac{L_{Wtotal}}{A\sigma} \quad (17)$$

$$P_{in} = P_{out} = P_{mech} + P_{heat} \quad (18)$$

$$\begin{aligned} P_{mech} &= \vec{F} \cdot \vec{d} \\ &= BIL \cdot d_{travel} \cdot f \end{aligned} \quad (19)$$

Combining equations 16, 17, 18 and 19 gives a formulation for temperature change of wires, assuming heat energy is conserved in wires:

$$\begin{aligned} P_{heat} &= P_{in} - P_{mech} \\ \rho Q c_{pWire} \Delta T &= \frac{I^2 L_{Wtotal}}{A\sigma} - BIL \cdot d \cdot f \\ \Delta T &= \frac{\frac{I^2 L_{Wtotal}}{A\sigma} - BIL \cdot d \cdot f}{\rho Q c_{pWire}} \end{aligned} \quad (20)$$

### 3.2 Optimisation Algorithm

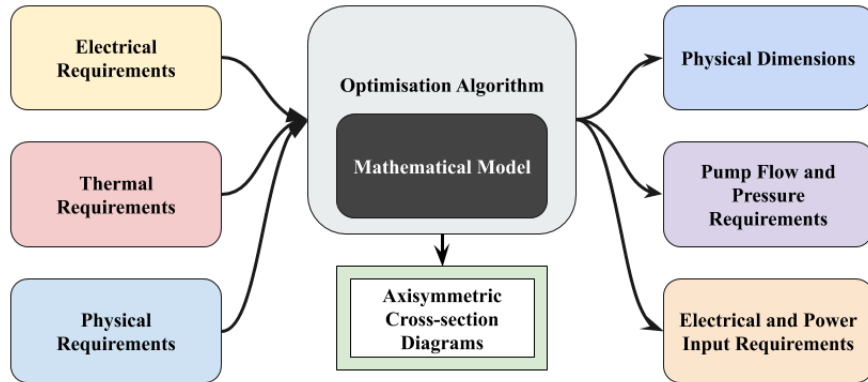


Figure 3: Diagrammatic representation of optimisation algorithm inputs and outputs

Grid-search optimisation for even numbered layers.

Optimised for an optimisation variable  $\mathcal{P}$ , which is the product of total motor mass and electrical input power.

Runs requirement checking function on each result and discards invalid solutions.

Optimisation was conducted assuming the use of 2 mm internal diameter, 3 mm external diameter silicone tubing for wiring. This was the tubing with largest internal volume to total volume ratio that was commercially available.

Table 1: Grid-search optimisation variables and units.

Variable	Units
Magnet length	m
Magnet radius	m
Core length	m
Bobbin length	m

Table 2: List of optimisation requirements and justifications.

Variable	Requirement	Justification
Output force	Must be over 9 N	Minimum to drive liquid metal pump
Acceptable temperature change in wires after circulation	Must be under 30 K	Higher temperatures may be a health and safety hazard
Travel distance of motor	Must be over 9 mm	Minimum to drive liquid metal pump
Bobbin length	Must be shorter than combined length of core and magnet	Not physically valid otherwise
Shell internal diameter	Must be under 80 mm	Not practical for manufacturing, assembly and handling if bigger
Total motor current	Must be under 10 A	No power supply available to drive more than 10 A
Total volume of wire	Must be under 15 ml	Limit to amount of eGaIn available and difficult to assemble with larger volume
Flow rate of liquid metal in wires	Must be positive	Validity check
Electrical power input	Must be positive	Validity check

The optimisation software produced physical dimensions, pump flow and pressure requirements, electrical input requirements and an axisymmetric cross-section diagram to show scale of the optimised motor for each number of layers that the optimisation was run for.

Choice between 4 layer design and 6 layer design

### 3.3 Design Validation

ANSYS Maxwell 2D electromagnetic simulation, axisymmetric about z-axis.

Table 3: Comparison between most efficient 4-layer and 6-layer motor designs.

Variable	4-layer solution	6-layer solution	Units
Magnet length	35	42.5	mm
Magnet radius	20	20	mm
Core length	12	8	mm
Bobbin length	27.5	23.75	mm
Shell internal radius	33.5	39.5	mm
Total wire length	6.68	9.55	m
Total wire resistance	0.15	0.22	$\Omega$
Minimum required current	7.75	6.27	A
Minimum required voltage	1.19	1.38	V
Minimum power input	9.22	8.63	W
Flow rate required for circulation cooling	0.135	0.125	$ml \cdot s^{-1}$
Pressure required to drive circulation cooling	5.51	7.28	kPa
Total mass of motor	1.21	1.50	kg
Optimisation Variable $\mathcal{P}$	11.19	12.98	$kg \cdot W$

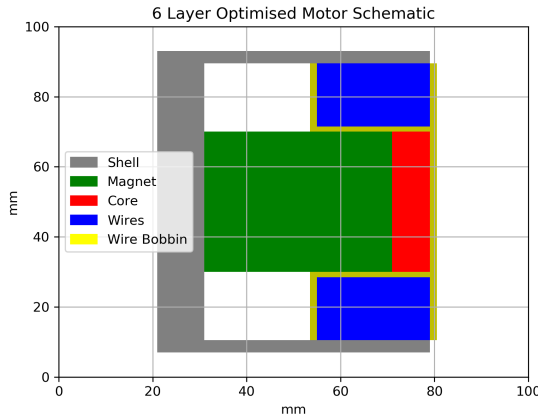


Figure 4: Cross-section diagram of final motor design

### 3.4 Physical Design and Manufacturing

4 axial, 40 mm diameter, 10 mm tall N45 grade neodymium disc magnets were used in series, to substitute for the required 40 mm diameter, 42.5 mm tall N42 grade neodymium magnet. The disc magnets also come with countersunk unthreaded M6 holes for fastening.

#### 3.4.1 Shell

Two-piece design, cylinder and base To enable safe assembly of magnets into motor M6 threads at centre of base to secure magnets and core Holes at end to secure spacer, and also enable ventilation while motor is in operation M3 threaded holes in side to secure

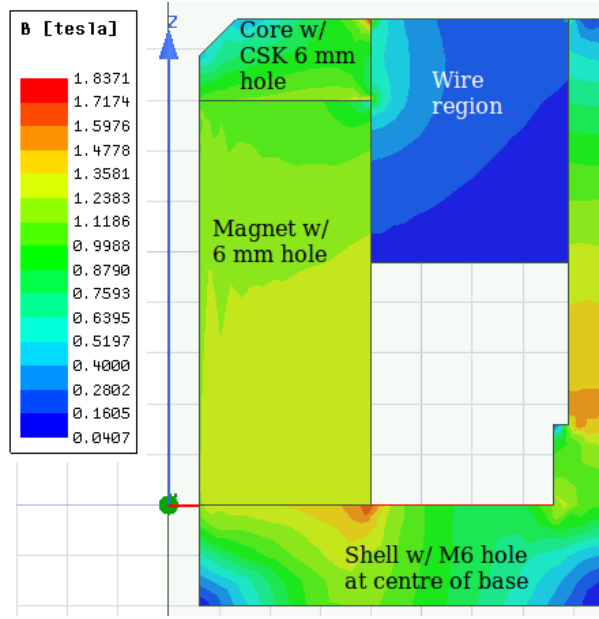


Figure 5: Maxwell 2D simulation of magnetic field density in motor

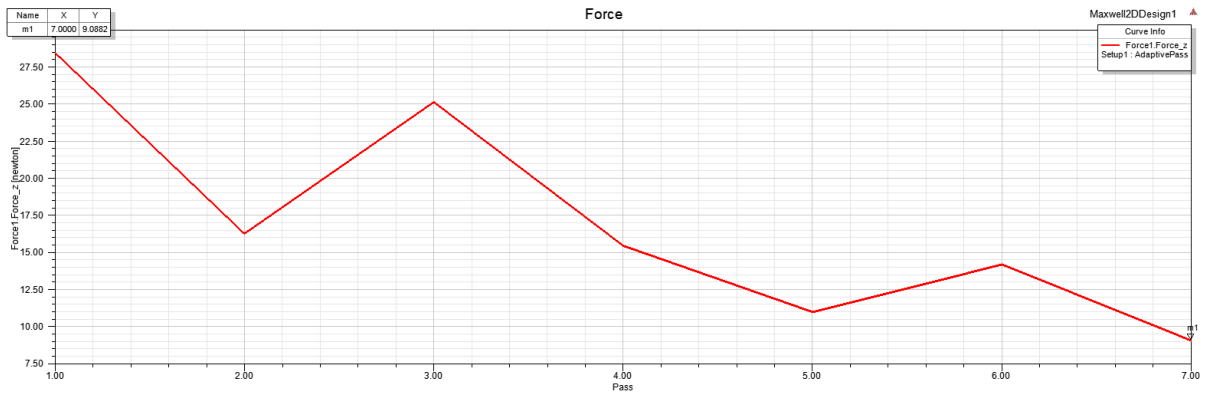


Figure 6: Convergence of force on wires to 9.0882 N in Maxwell 2D simulation

shell cylinder during assembly step that attaches base, magnets and core to cylinder. Both turned on lathe from 1020 grade 100 mm diameter engineering bar steel stock

### 3.4.2 Core

8 mm thick, 40 mm diameter cylinder with countersunk unthreaded M6 hole in the centre. A bolt travels through the hole that secures the core to the magnets to the shell base.

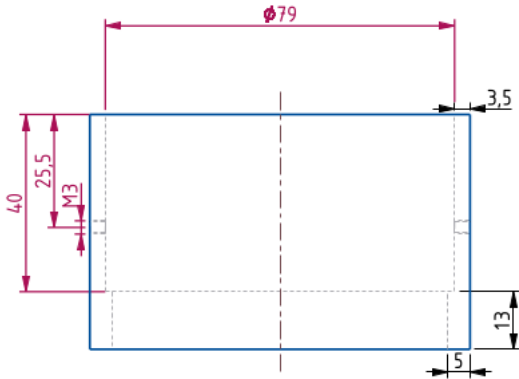


Figure 7: Axisymmetric cross-section drawing of final shell cylinder



Figure 8: Axisymmetric cross-section drawing of final shell base. Units in mm.

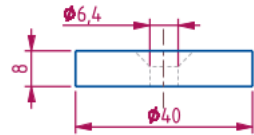


Figure 9: Axisymmetric cross-section drawing of final core. Units in mm.

### 3.4.3 Wire Bobbin

## 3.5 Assembly

### 3.5.1 Shell and Magnet Assembly

### 3.5.2 Wire Assembly

### 3.5.3 Health, Safety and Containment

Gallium, indium and eGaIn are not toxic to touch, but can cause harm if ingested or inhaled.

However, eGaIn is known to be corrosive towards most solid metals including iron, copper and aluminium alloys [9]. In particular, without specific surface treatment, aluminium parts in the lab may corrode on contact with eGaIn.

Everything done in fish bin, done in a corner of the lab away from metal components that can be damaged.

To avoid accidental ingestion after handling eGaIn, disposable gloves were worn whenever there was possible exposure to eGaIn.

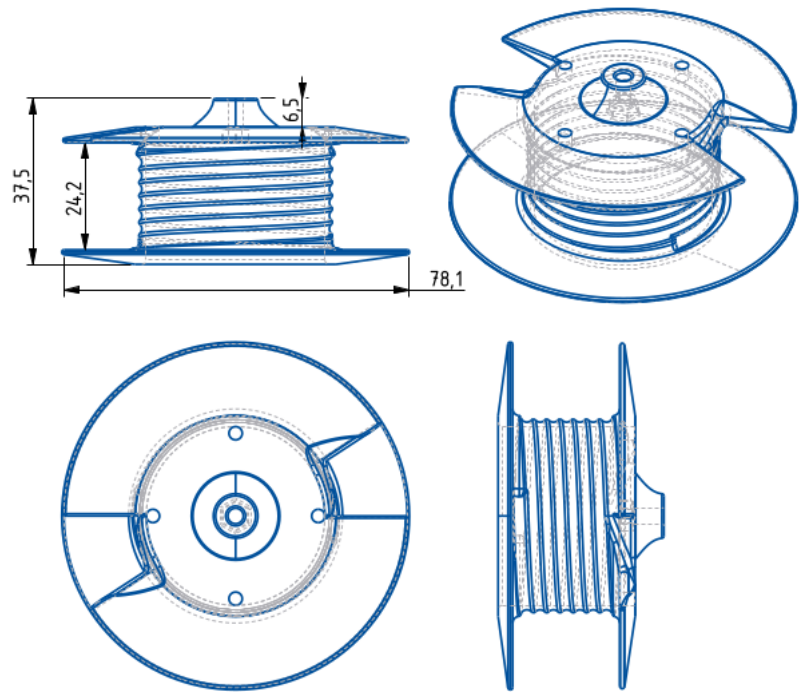


Figure 10: Three-view drawing of final wire bobbin. Units in mm.

**\*\*\*Placeholder\*\*\***

Figure 11: Contraption used to safely assemble magnets and core onto shell base.

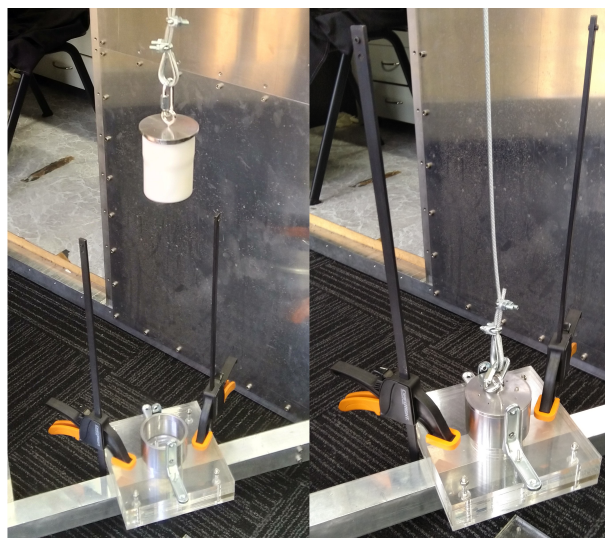


Figure 12: Shell base with magnets and core attached being lowered onto shell cylinder.

## 4 Experiment Designs and Results

### 4.1 Experiment 1: Force Characterisation

#### 4.1.1 Method

Plate on bobbin, motor oriented vertically. 15



Figure 13: Assembled shell with magnets and core attached.

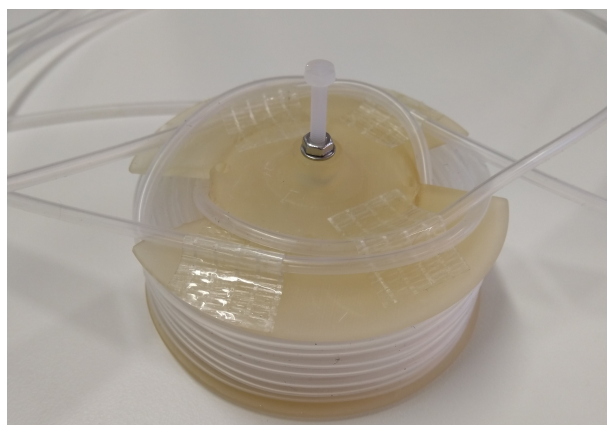


Figure 14: Bobbin with complete silicone tube windings. Tubes wound by hand.

\*\*\*Placeholder\*\*\*

Figure 15: Experiment setup to characterise force output of motor given different electrical input.

#### 4.1.2 Results

### 4.2 Experiment 2: Circulation Thermoregulation

#### 4.2.1 Method

#### 4.2.2 Results

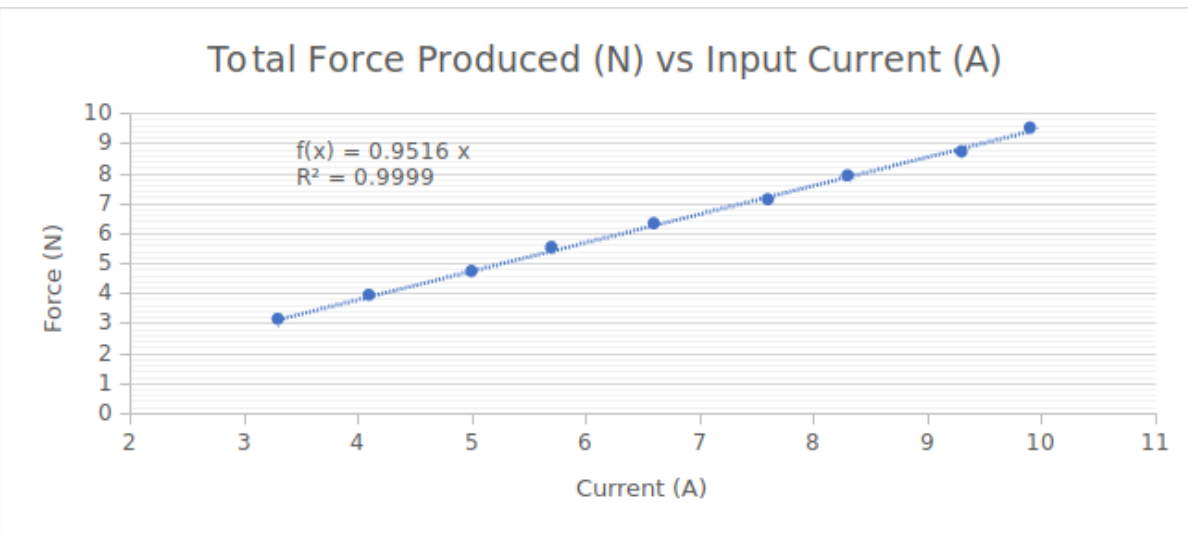


Figure 16: Experimental result motor force plotted against provided current.

Table 4: Analysis of force experiment results.

Item	Value	Units
Average efficiency ex. Bobbin	1.00	$NA^{-1}$
Mass of bobbin & fixed cup	335.22	g
Current required for 9 N	8.75	A
Theoretical current for 9 N	8.50	A

## 5 Discussion

Application to the original physical situation

Comparison with related problems and other solutions

If the eGaIn in the final motor design was substituted for copper threaded through silicone tubing, the motor would require much less power to produce the same force output. A motor of the same size filled with copper coils of the same diameter instead of eGaIn will consume under half of the power for the same force output. If the volume of the wiring was substituted entirely for 0.22 mm diameter copper wire, a common type of wire used for electromagnetic motors of this force scale, the motor would draw 18 times less power to produce the same force.

Critical assessment of significance

Difficulty of the problem and how well it has been tackled

Table 5: Comparison between final eGaIn motor and two hypothetical solutions using copper wiring.

Variable	eGaIn solution	Copper equal	Copper fill	Units
Total wire length	9.55	9.55	157.76	<i>m</i>
Total wire resistance	0.22	0.026	34.86	$\Omega$
Required current	6.27	6.27	0.12	<i>A</i>
Power input	8.63	3.12	0.46	<i>W</i>

## 6 Conclusion

## 7 Appendices

### 7.1 Full Results of Motor Force Experiment

Table 6: Results from motor force experiment.

Number of Weights	Mass Balanced (g)	Incremental Total Mass Balanced (g)	Total Force (N)	Voltage (V)	Current (A)	Power (W)
0	335.22†	335.22	3.29	1.57	3.30	5.18
1	81.53	416.75	4.09	1.96	4.10	8.04
2	81.11	497.86	4.88	2.36	5.00	11.80
3	81.32	579.18	5.68	2.72	5.70	15.50
4	81.12	660.30	6.48	3.05	6.60	20.13
5	81.65	741.95	7.28	3.45	7.60	26.22
6	81.19	823.14	8.07	3.68	8.30	30.54
7	81.43	904.57	8.87	4.07	9.30	37.85
8	80.65	985.22	9.66	4.35	9.90	43.07

†Estimated using average efficiency, seen in table 4 calculated from incremental current required to produce incremental force, both seen in table 7.

Table 7: Incremental values between adding each additional weight during motor force experiment‘.

Number of Weights	Force increment (N)	Current increment (A)	Incremental Efficiency (N/A)
0	3.29	3.30	1.00
1	0.80	0.80	1.00
2	0.80	0.90	0.88
3	0.80	0.70	1.14
4	0.80	0.90	0.88
5	0.80	1.00	0.80
6	0.80	0.70	1.14
7	0.80	1.00	0.80
8	0.79	0.60	1.32

## References

- [1] Engineering ToolBox. (2016). Permeability, [Online]. Available: [https://www.engineeringtoolbox.com/permeability-d\\_1923.html](https://www.engineeringtoolbox.com/permeability-d_1923.html) (visited on 09/22/2019).
- [2] R. Baartman, *Materials library in FEMM 4.0*, May 19, 2007.
- [3] S. W. Jin, J. Park, S. Y. Hong, H. Park, Y. R. Jeong, J. Park, S.-S. Lee, and J. S. Ha, “Stretchable Loudspeaker using Liquid Metal Microchannel”, *Scientific Reports*, vol. 5, p. 11695, Jul. 16, 2015, ISSN: 2045-2322. DOI: 10.1038/srep11695. [Online]. Available: <https://www.nature.com/articles/srep11695> (visited on 04/28/2019).
- [4] M. D. Dickey, R. C. Chiechi, R. J. Larsen, E. A. Weiss, D. A. Weitz, and G. M. Whitesides, “Eutectic Gallium-Indium (EGaIn): A Liquid Metal Alloy for the Formation of Stable Structures in Microchannels at Room Temperature”, *Advanced Functional Materials*, vol. 18, no. 7, pp. 1097–1104, 2008, ISSN: 1616-3028. DOI: 10.1002/adfm.200701216. [Online]. Available: <http://onlinelibrary.wiley.com/doi/10.1002/adfm.200701216> (visited on 05/03/2019).
- [5] R. Houghton, “Hazards”, in *Emergency Characterization of Unknown Materials*, CRC Press, Oct. 15, 2007, p. 89, ISBN: 978-0-8493-7969-7.
- [6] T. Liu, P. Sen, and C. Kim, “Characterization of Nontoxic Liquid-Metal Alloy Galinstan for Applications in Microdevices”, *Journal of Microelectromechanical Systems*, vol. 21, no. 2, pp. 443–450, Apr. 2012, ISSN: 1057-7157. DOI: 10.1109/JMEMS.2011.2174421.
- [7] E. Coates. (Dec. 22, 2018). Transformer Cores, Reluctance and Permeability, [Online]. Available: [http://www.learnabout-electronics.org/ac\\_theory/transformers02.php](http://www.learnabout-electronics.org/ac_theory/transformers02.php) (visited on 09/22/2019).
- [8] T.-H. Chang, “Chapter 7: Electrodynamics”, Dec. 21, 2006, [Online]. Available: <http://www.phys.nthu.edu.tw/~thschange/notes/EM07P1.pdf> (visited on 09/22/2019).
- [9] Y. Cui, Y. Ding, S. Xu, Z. Yang, P. Zhang, W. Rao, and J. Liu, “Liquid Metal Corrosion Effects on Conventional Metallic Alloys Exposed to Eutectic Gallium-Indium Alloy Under Various Temperature States”, *International Journal of Thermophysics*, vol. 39, no. 10, p. 113, Aug. 20, 2018, ISSN: 1572-9567. DOI: 10.1007/s10765-018-2440-x. [Online]. Available: <https://doi.org/10.1007/s10765-018-2440-x> (visited on 09/22/2019).
- [10] J. Liu, “Liquid metal machine is evolving to soft robotics”, *Science China Technological Sciences*, vol. 59, no. 11, pp. 1793–1794, Nov. 1, 2016, ISSN: 1869-1900. DOI: 10.1007/s11431-016-0696-7. [Online]. Available: <https://doi.org/10.1007/s11431-016-0696-7> (visited on 05/02/2019).